TRIBOLOGIA - Finnish Journal of Tribology 1-2 vol 40/2023

https://doi.org/10.30678/fjt.127844

SUOMEN TRIBOLOGIAYHDISTYS RY
THE FINNISH SOCIETY FOR TRIBOLOGY
www.tribologysociety.fi
https://journal.fi/tribologia

Prediction Of The Coefficient Of Friction In The Single Point Incremental Forming Of Truncated Cones From A Grade 2 Titanium Sheet

Tomasz Trzepieciński[1] and Marcin Szpunar[2*]

[1]Department of Manufacturing Processes and Production Engineering, Faculty of Mechanical Engineering and Aeronautics, Rzeszow University of Technology, al. Powstańców Warszawy 8, 35-959 Rzeszów, Poland

[2]Doctoral School of Engineering and Technical Sciences at the Rzeszów University of Technology, Rzeszów University of Technology, al. Powst. Warszawy 12, 35-959 Rzeszów

Corresponding author: Marcin Szpunar (d547@stud.prz.edu.pl)

ABSTRACT

The aim of this paper is to analyze the effect of the process parameters on the coefficient of friction (COF) in the single-point incremental forming process. This investigation may be useful for further FEM analyses where the tool -workpiece contact must be set appropriately to obtain adequate results. The friction was analyzed between a solid tungsten carbide ⌀8 hemispherical ended tool with a radius of 4 mm and a grade 2 pure titanium sheet. As a lubricant, 10W40 engine oil was used. The experiment was of a central composite design and 20 runs in random order were carried out. The influence of input factors, namely spindle speed, tool feed and incremental step depth, was analyzed for the COF response. Two type of equations founded in the literature have been acquired to calculate COF values. An investigation of COF analysis was done for initial tool contact, the first tool full depth contact and stabilized forming region. Additionally, single components of the horizontal force (X-axis and Y-axis) were taken into account. Analysis of variance shows that there is no correlation between the input factors and the COF responses. However, the mean model fitted to the results obtained allows for the prediction of the COF by using the vertical force component and only one horizontal force component. The resulting mean value of the COF between the tool and the workpiece equals 0.4 for Eq. (1) initial contact, stabilized forming: Eq. (1) 0.656 and Eq. (2) 0.469.

Keywords: single point incremental sheet forming; coefficient of friction; titanium sheet; solid tungsten carbide

1. Introduction

Titanium alloys are widely used in aerospace, automobile, orthopaedic and dental applications because of their excellent corrosion resistance and high strength to weight ratios. Single point incremental forming (SPIF) is a flexible forming process with a lot of benefits compared to conventional sheet forming. The SPIF of titanium and its alloys plays an important role in modern manufacturing techniques, enabling the production of complex forms at low production costs [1]. A universal toolkit allows different shapes to be obtained, which leads to flexibility in production and a reduction in tooling costs. In addition, it is possible to achieve a greater strain. However, this process is only profitable in small batch production when forming metallic [2,3], polymer [4] and composite [5,6] sheets. The main advantages of SPIF include [7,8]: the possibility of forming elements on a conventional CNC machine (lathe or milling machine) and quick and easy changes to the geometry of the formed elements.

In the SPIF process, the round-shaped forming tool gradually forms the sheet by making an integrated movement around the fixed edge of the workpiece. Then, the tool makes an in-depth movement by a specified step size ap and forms the shape of the component by moving along the next horizontal trajectory with a feed rate f [9,10]. In SPIF, friction plays a crucial role in tool-workpiece contact [11]. Friction not only affects the formation limit, but also affects the surface quality of the formed parts [12-14]. Surface quality is given serious attention in metal construction because it affects not only the aesthetic appearance of the components, but also the performance and life span.

The lubricants used during SPIF correspond to those used in conventional sheet forming processes and are mainly adapted to the pressure values, the material grade of the workpiece–tool material pair and the tool rotational speed [15,16]. Among the many factors affecting the possible use of the incremental sheet forming (ISF) method and forming accuracy, the technological parameters (e.g., tool diameter, step size, tool rotational speed, friction conditions), mechanical parameters of the workpiece (e.g., work hardening, anisotropy of the material, Young's modulus) and factors resulting from the product design (e.g., sheet thickness, geometry of drawpiece) [17,18] should be indicated. Higher rotational speeds of the tool allow the application of greater plastic deformations of the sheet material without the risk of cracking and are used to form thin sheets with limited plasticity [19,20].

Table 1. Chemical composition of the test material (wt.%)

O	Fe	N	C	Ti
0.23	0.12	0.009	0.009	balance

Table 2. Basic mechanical properties of grade 2 pure titanium sheets

ASTM	Density, g/cm3	Delivery condition	Modulus of elasticity, GPa	Yield strength, MPa	Ultimate tensile strength, MPa
Grade 2	4.50	Annealed	100	330	430

Table 3. Selected properties of the material selected for the forming tool

Grade (ISO)	Density, g/cm3	Tungsten carbide, %	Co, %	Grain size, μm	Bending strength, MPa	Hardness HV30
K30-K40	14.45	90	10	0.6	3600	1610

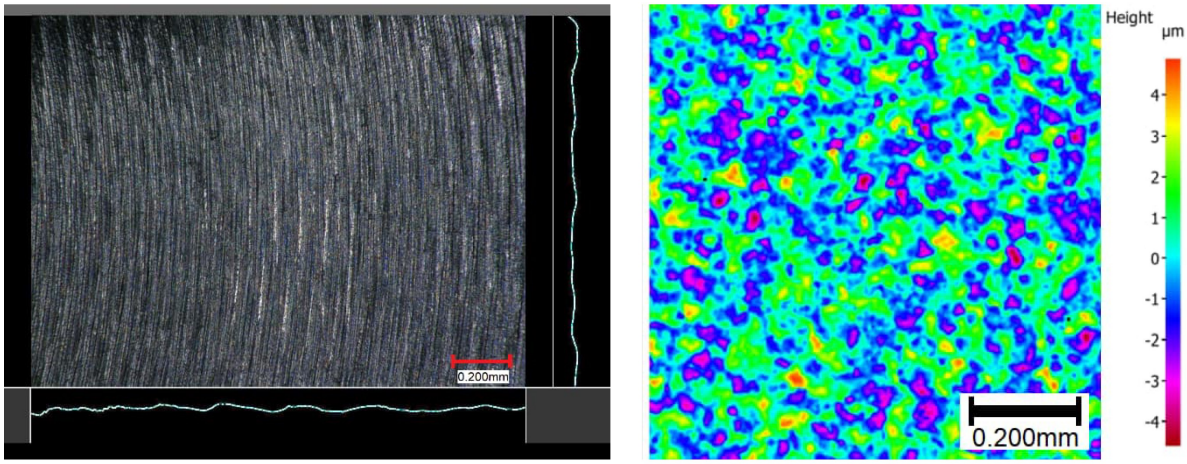

(a) (b)

Figure 1. Surface roughness results: a) forming tool tip at radius, b) titanium sheet blank.

The problem of ensuring appropriate forming conditions is related to the contact of a relatively low strength with a tool of high hardness and strength [21]. Lubricants differ in many characteristics, such as consistency (i.e., liquid, paste), density and viscosity. Gulati et al. [22] studied the SPIF of EN AW-6063 aluminium alloy sheets under conditions of dry friction, lubrication with solid grease and with the use of a cutting-tool lubricant. Using the analysis of variance, the process parameters affecting the surface roughness of the drawpieces were determined. It was found that solid grease significantly affects the roughness of the product compared to forming in dry friction conditions. In the case of rubbing of rough surfaces, the solid lubricant forms a layer between the tool and the sheet, limiting the metallic contact of the surface asperities [22]. Wei et al. [23] studied the effects of processing on the roughness of the interior surface and the friction indicator on the interface of the tool/sheet during the incremental forming of the aluminium sheets. The results of the analysis show that the friction and roughness indicators are similar in response to changes in the input parameters. Furthermore, a relationship between coefficient of friction and the surface has been presented by the authors. In their work, the greater the COF the higher the surface roughness. However, there is a lack of extended research in the this kind of topic in case of SPIF. Cai et al. [24] investigated numerical simulations in ABAQUS with experimental validation. The authors found that the coefficient of friction (COF) affects the temperature in the forming zone. The greater the COF, the higher the temperature of the tool. Based on the results of grey relational analysis, Patel et al. [25] conclude that solid lubricant plays a key role in SPIF at low spindle speeds, while liquid lubricant is preferred at high spindle speeds. Studies of the effect of several lubricants on the surface finish quality of EN AW-1050-T4 aluminium alloy drawpieces show that the greater the hardness of the sheet material, the lower the viscosity of the lubricant required. Xu and Yao [26] applied a Box-Behnken design to examine the effect of input factors such as tool diameter, layer feed, spindle speed, feed speed and forming angle on the COF response. The authors carried

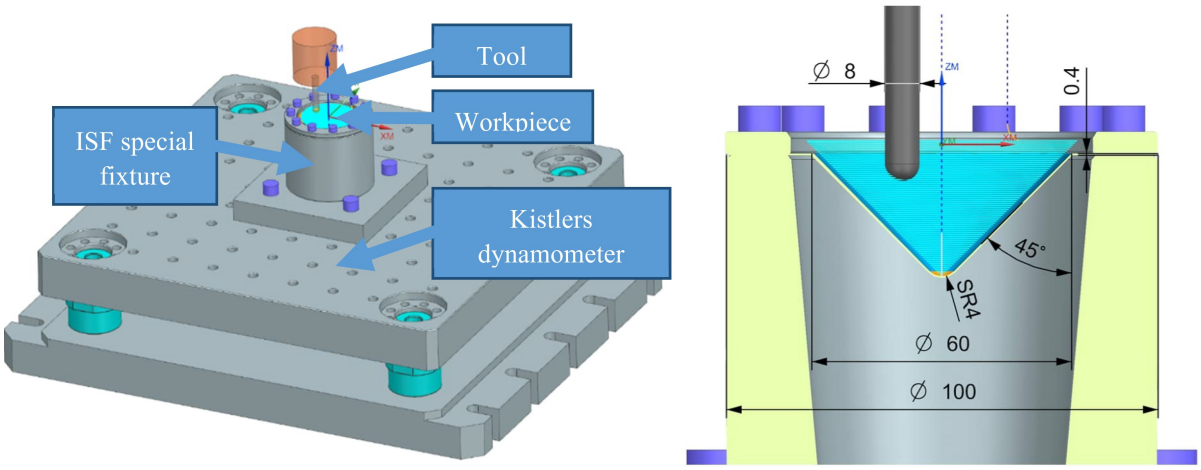

Figure 2. a) Test stand dedicated to measuring force during the incremental forming process, b) CNC path with drawpiece dimensions (in mm).

Table 4. Experiment range for the input factors

Factor name	Coded	Low value	High value
Spindle speed v, rpm	A	-600	600
Feed rate f, mm/min	B	500	2000
Incremental step depth a_p, mm	C	0.1	0.5

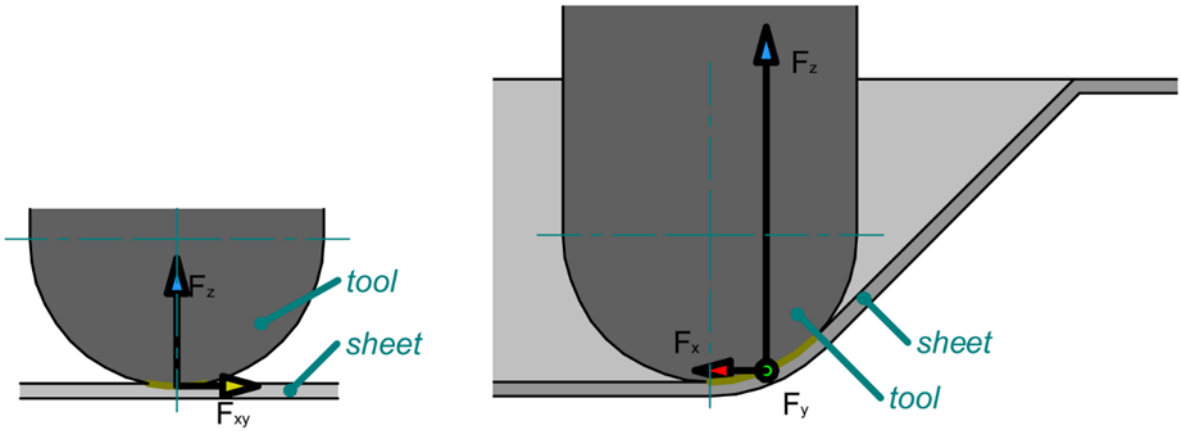

Figure 3. Force components during: a) initial contact stage (Fz=40-60 N) b) stabilized forming.

out 46 SPIF runs for EN AW-1060 sheets formed using a solid carbide hemispherical tool. Furthermore, the COF results were imported into a finite element model and validated. Due to the high-accuracy of Kistler measurement equipment, the experimental force results were similar to those from finite element-based computations. The authors propose a regression model that describes the response of COFs to input factors, with the tool diameter being the most influential. Najm and Paniti [27] used an artificial neural network to explore and determine the formability of the workpiece and the geometry of the forming tools. They also determined an analytical equation for each output based on the extracted weight and bias of the best network prediction. The characteristics of the tools were found to play an essential role in all predictions and fundamentally impact the final products. Najm et al. [16] studied the diameter of the effects of the forming tool, the speed of the tool, the feed rates and the type of coolant on the hardness of EN AW-1100 aluminium alloy sheets in SPIF. The effects of various coolant oils and greases were studied using the same feed rates. It was found that when a coolant oil was used, the hardness increased, and when grease was applied, the hardness decreased. Pepelnjak et al. [28] manufactured a X6Cr17 stainless steel denture base plate of a complete maxillary denture to replace a traditional prosthodontic procedure based on a lost-wax technique. Conventional mineral oil was used as the lubricant. The experimental tests related to the surface roughness of the inner surface of the drawpiece show a significant influence of step size on

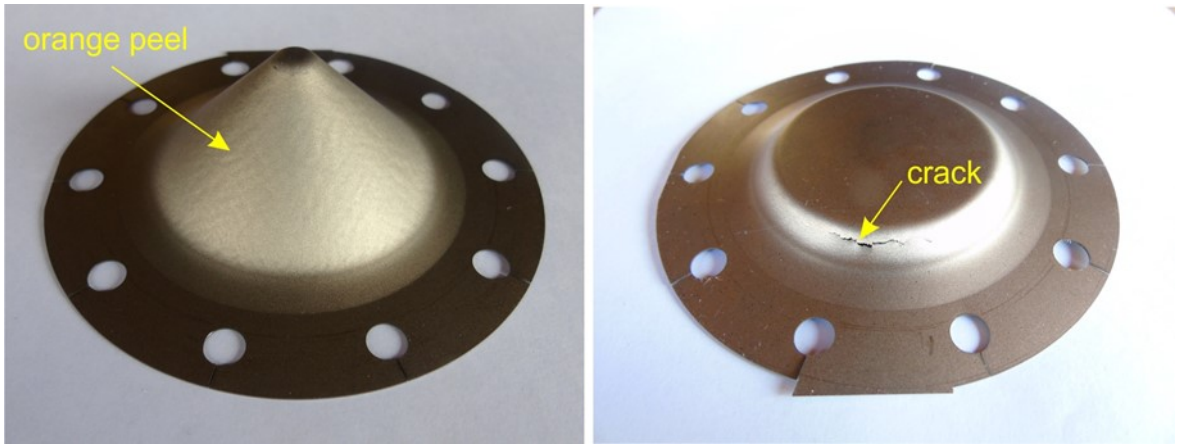

Figure 4. (a) A successfully formed drawpiece (run 12) and (b) a failed drawpiece (run 15)

the surface quality. Sbayti et al. [29] investigated the SPIF process of a Ti6Al4V titanium alloy acetabular cup at high temperature using FE-based simulations and an optimization procedure. The effects on the final part of four key process parameters, particularly the COF, the processing temperature, the step depth and the tool diameter, were analyzed. The computational results prove that moth-flame optimization, multiverse optimization and Harris Hawk optimization are very competitive in geometry optimization. Popp et al. [30] studied the sheet metal bending mechanism in the SPIF of AlCu4PBMgMN aluminium alloy drawpieces using an FE-based method analysis. It was found that the shape of the retaining rings has a large influence on the final geometrical accuracy of the parts manufactured using SPIF. Rosca et al. [31] conducted an experimental study on the effect of the main technological factors, such as vertical step and the tool diameter, on the robotized SPIF of A3 deep-drawing steel sheets. They estimated the effect of the tool diameter and vertical step on thickness reduction and springback and found that the springback increases with an increasing vertical step but is less influenced by the tool diameter.

Many of the research focuses on incremental sheet-forming parameter optimization for pure titanium sheets. Hussain et al. [32] found that an increase in feed rate or incremental step depth decreases formability, while a greater tool diameter improves. Veera ajay [33] confirmed that those input factors seem to be the most influential on process parameters such as surface roughness, wall angle and thickness. Elevated tool relative velocity has been found to be important for the formation of forces and for the formation success (without crack) [34]. Other researches focus on microstructure effect after SPIF pure titanium sheets. Kumar et al. [35] investigated the magnitude and state of residual stresses after the forming process for a commercially pure titanium grade 2. They found that with increasing wall angles and incremental step depth, the residual tensile stresses became higher. Mishra et al. [36] analyzed microstructure and texture evolution, found that prismatic slip is dominant for SPIF pure titanium, while the occurrence of twinning depends on many parameters and is heterogeneous. The effect of tool rotation on the mechanical properties and microstructure was analyzed by Yoganjaneyulu et al. [37]. The authors founds that grain orientation and elongation is along incremental step depth and tool rotation does not effect to grain size. However, elevated rotation of the tool causes strain hardening effect by increasing the density of dislocations.

Literature analysis shows that research on SPIF of pure titanium sheets is mainly focused on determining the influence of input parameters on the geometrical accuracy and mechanical properties of the drawpieces. Studies of friction conditions in SPIF quantified by the value of the COF are niche. Therefore, in this research paper, the influence of basic SPIF input parameters, namely spindle speed, tool feed rate and incremental step depth, on the COF between a solid carbide hemispherical tool and grade 2 titanium sheet has been investigated.

2. Materials and Methods

Friction analysis during the SPIF process has been investigated between a commercially pure titanium grade 2 sheet and a tungsten carbide grade ISO K30-K40 tool. Ultra-micrograin K30-K40 grade with high toughness is particularly recommended for rotating tools for the machining of titanium and titanium alloys. The workpiece sheet was produced by Timet (Toronto, OH, USA). The chemical composition of the sheet metal material based on the manufacturer's card is listed in Table 1. The initial sheet thickness was 0.4 mm and its basic mechanical properties are presented in Table 2. The tool was made of an 8 mm diameter rod with a hemispherical end with a radius of 4 mm. Table 3 presents the selected properties for the tool material provided by the manufacturer. The surface roughness of the hemispherical forming tool (Fig. 1a) and titanium sheet blank (Fig. 1b) were measured before the forming experiment by using Keyence Digital Microscope VHX-7000. The surface parameters are: Sa = 1.36 μm, Sz = 11.77 μm for hemispherical tool tip and Sa = 1.27 μm, Sz = 9.67 μm for as-received sheet blank.

A 3-axis Makino PS95 CNC milling machine was selected to carry out the experiment. The sheets were clamped in a special fixture located on a Kistler

Table 5. The experiment's input factors with COF response values.

Run	A: Spindle speed v, rpm	B: Feed rate f, mm/min	C: Incremental step depth a_p, mm	COF Eq. (1) Initial contact	COF Eq. (1) Stabilized forming	COF Eq. (2) Stabilized forming	COF Eq. (1) Xmax	COF Eq. (1) Ymax
1	0	1250	0.563	0.56	crack	crack	crack	crack
2	0	1250	0.300	0.39	crack	crack	crack	crack
3	790	1250	0.300	0.38	0.62	0.43	0.65	0.64
4	-200	1250	0.300	0.33	0.72	0.54	0.72	0.73
5	200	2237	0.300	0.3	crack	crack	crack	crack
6	200	1250	0.300	0.34	crack	crack	crack	crack
7	-790	1250	0.300	0.4	0.66	0.47	0.63	0.61
8	0	1250	0.037	0.51	crack	crack	crack	crack
9	0	263	0.300	0.37	crack	crack	crack	crack
10	400	1250	0.300	0.37	0.65	0.46	0.65	0.64
11	600	500	0.500	0.34	0.65	0.46	0.66	0.66
12	-600	500	0.500	0.41	0.6	0.40	0.61	0.61
13	-400	1250	0.300	0.44	0.69	0.51	0.72	0.71
14	600	2000	0.500	0.28	0.63	0.44	0.64	0.64
15	600	2000	0.100	0.49	crack	crack	crack	crack
16	600	500	0.100	0.31	0.63	0.44	0.66	0.67
17	-600	2000	0.100	0.42	0.64	0.45	0.65	0.67
18	0	1250	0.300	0.44	crack	crack	crack	crack
19	-600	500	0.100	0.43	0.67	0.49	0.7	0.69
20	-600	2000	0.500	0.48	0.71	0.53	0.74	0.74

dynamometer table to measure the process outputs of the 3 -axis forces (Figure 2a). A conical frustum drawpiece with a wall angle of 45° was determined as the shape of the specimen (Figure 2b). A 10W-40 semi-synthetic oil was deposited to improve lubrication between the tool and the workpiece.

The ranges for the parameters in the experiment (Table 4) were determined by the literature review and preliminary trials. A central composite design was selected as the experiment plan. As input factors, spindle speed, tool feed and incremental step depth were determined, which resulted in the 16 runs presented in Table 5 (14 runs on the corners, two points in the cube center). An additional four runs were included in the experiment to accurately describe the effect of the influence of tool rotation. Siemens NX PLM software was used to generate the model geometry, then to create the CNC path and finally the CNC file for the milling machine. Twenty planned drawpieces were formed in the SPIF process, one by one in a randomly generated order.

The value of the friction coefficient was determined according to the following equation [38, 39]:

$$\mu = \frac{\sqrt{F_x{}^2 + F_y{}^2}}{\sqrt{F_z{}^2}} \tag{1}$$

where: F_x and F_y are the horizontal (in-plane) components of the forming force and, F_z is the axial components of the forming force.

Equation (1) enables the prediction of the COF by entering the axial and horizontal forces during the SPIF process. This equation has been widely used by many researchers. Shin [40] in his dissertation presented that the friction coefficient does not affect axial force more than 10% by FEM analysis. However, the higher the COF, the greater horizontal forces were observed. Durante et al. [41] carried out COF using this equation in sliding tests between an ISF tool and 20 mm wide specimens. Hamilton [42] in his thesis work obtained the same equation, which

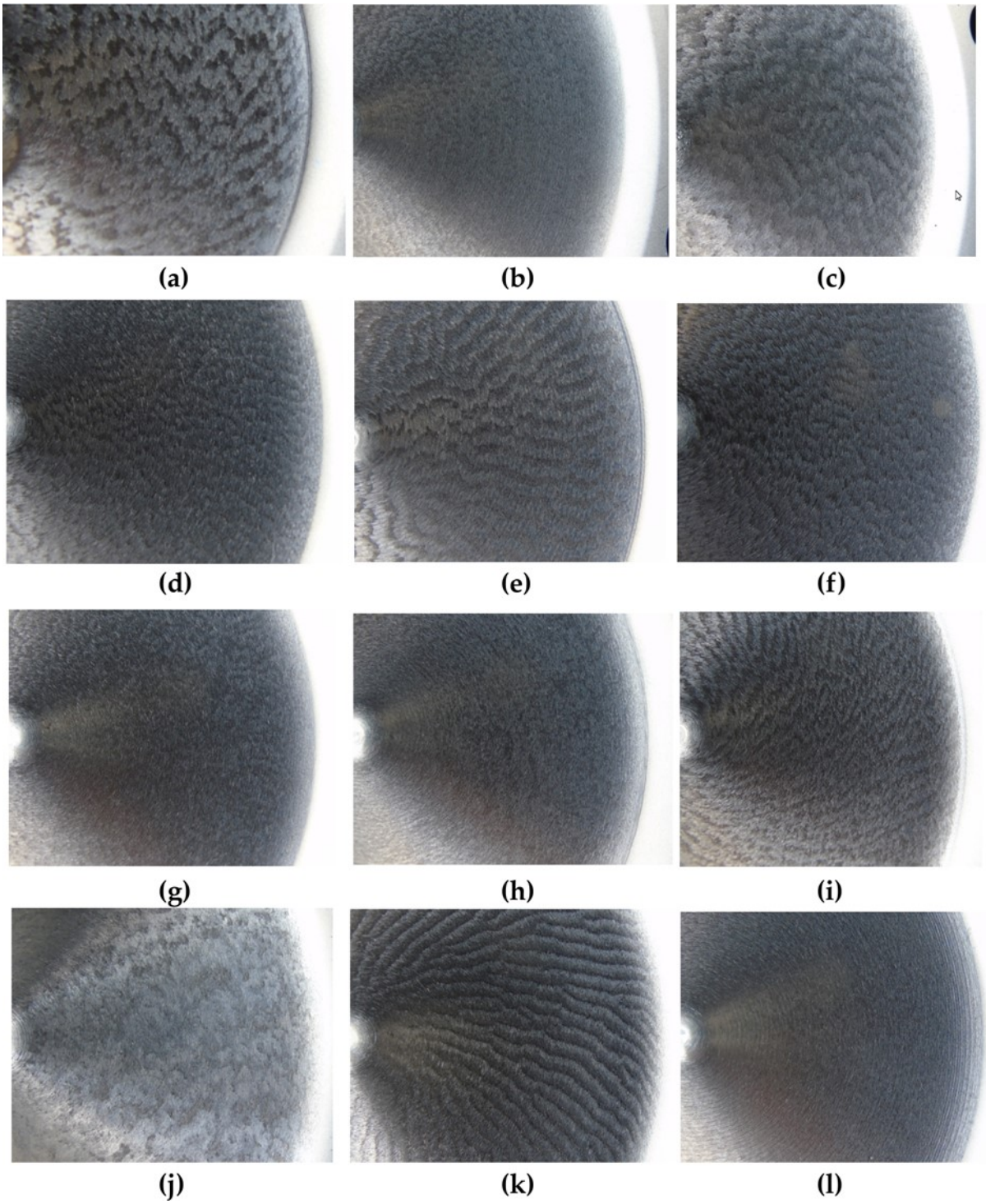

Figure 5. View of the inner surface of the drawpieces for run numbers (a) 3, (b) 4, (c) 7, (d) 10, (e) 11, (f) 12, (g) 13, (h) 14, (i) 16, (j) 17, (k) 19, (l) 20

was further applied and successfully confirmed with FEM analysis by Li et al. [43].

Equation (1) has been applied to the early stage of forming where the horizontal force component (Fxy) is responsible for the friction, while the axial force component (Fz) represents the normal reaction (Fig 3a). The data obtained from the dynamometer was filtered to the range where the axial component equals from 40-60 N. From the filtered range, Eq.(1) was applied, then the mean of the results was taken to further analysis. In addition, a trial of COF investigation by Eq.(1) was also prepared for the tool full depth plunge and stabilized forming region. Such a calculation may be inaccurate due to the fact that some part of the horizontal component is also responsible for the normal reaction rather than friction (Fig. 3b). Separate analyses have been carried out for stabilized forming region by independently selecting the maximum single component of the horizontal force for the X and Y

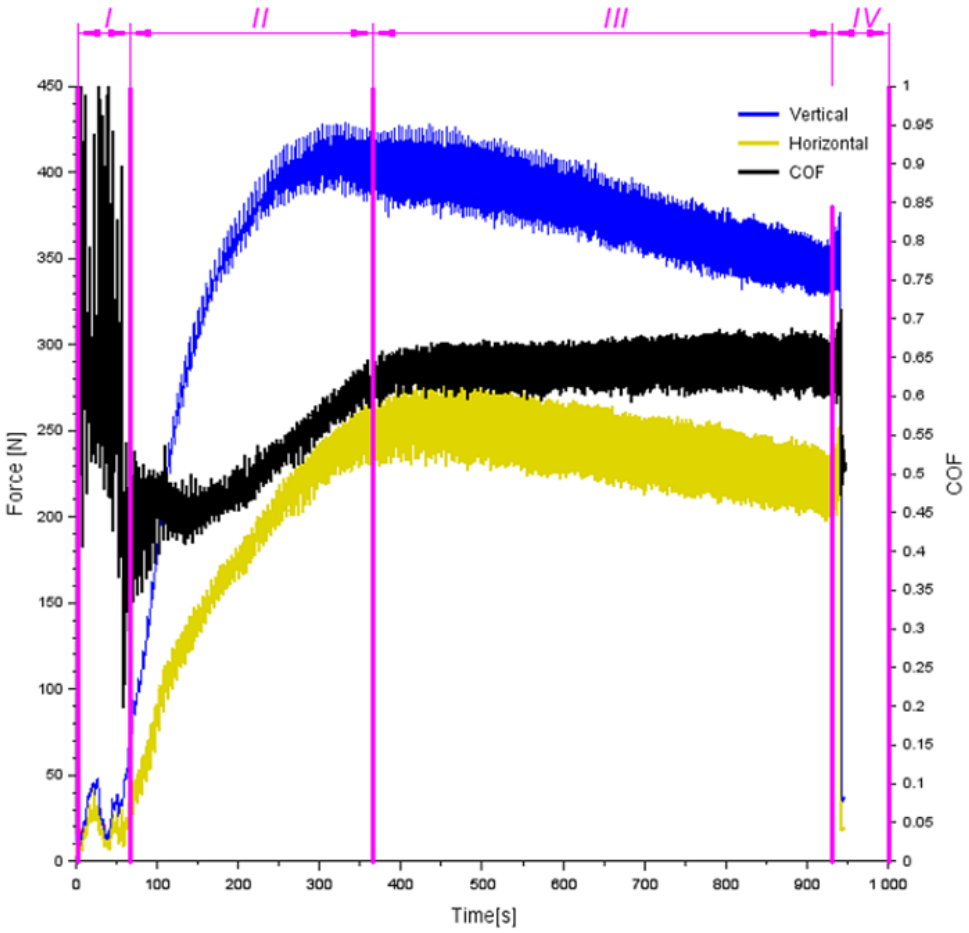

Figure 6. Forces outputs and COFs Eq. (1) calculated for the formation time (run 17): I – tool approach stage, II – stabilization of the forming process, III– stable forming zone, IV – tool retraction stage

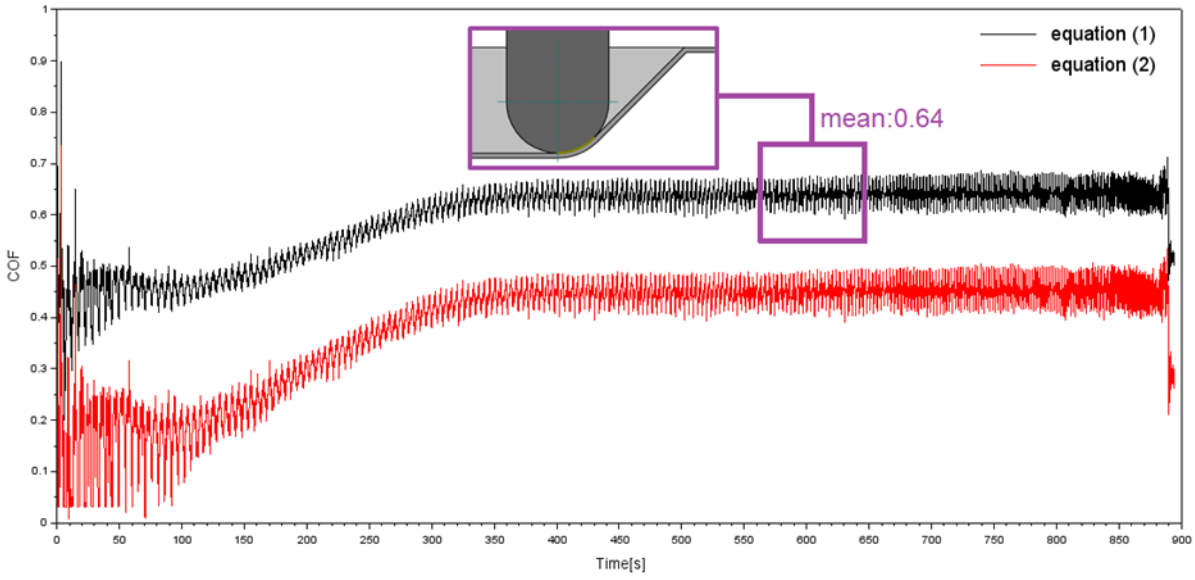

Figure 7. Comparison between two equations (1) and (2) that describe the friction coefficient during the SPIF process for run #17 with a COF read for stabilized forming region.

axes.

The equation proposed by Xu et al. [44] was also used as a comparison for the stabilized forming region. The authors proposed a calculation where the angle of the drawpiece wall angle (α) is included and the relationship between the horizontal and vertical force can be estimated by:

$$\mu = \sqrt{\frac{\left(F_x^2 + F_y^2\right) \times \cos^2\frac{\alpha}{2}}{F_z^2} - \sin^2\frac{\alpha}{2}} \quad (2)$$

where: F_x and F_y are the horizontal (in-plane) components of the forming force and, F_z is the axial components of the forming force and α is the angle of the cone - in current experiment 45°.

3. Results and Discussion

Table 5 presents the values of the COF determined for individual experiments. The average COF for the stabilized region is between 0.6 and 0.74 for Eq. (1) and 0.43 and 0.54 for Eq. (2) respectively. A crack mainly occurred in the bottom zone of the drawpiece (Figure 3b), where the material was the thinnest and most work hardened. The properly shaped drawpieces were characterized by an outer surface with an 'orange peel' effect (Figure 4a). Orange peel is a surface defect that occurs in SPIF when the tool is in intimate contact with one side of the workpiece. Due to the anisotropic character of the sheet metal fabricated in a rolling process, neighboring grains at the surface tend to thicken or thin differently, giving a roughened look.

Although the COF values were in a similar range of between 0.6 and 0.74, significantly different inner surfaces of the drawpieces were obtained (Figure 5). The results show that the complexity and roughness of the formed surfaces changed with changes in the input parameters. The formation of characteristic surfaces, which can be described by fractal theory [45], can be explained by the fact that the increase in step size may have different effects on the surface. Increasing the step size can cause chatter due to the higher rate of strain, increasing the complexity of the surface texture. However, a higher incremental step depth results in step marks on the surface with a larger step distance. A higher feed rate results in a larger pitch spacing of the marks on the deformed surface. A lower feed rate results in the formation of machining traces with a smaller height. On the other hand, marks with greater height are moderated by a combination of high incremental step depth and feed rate. The highest surface uniformity was observed for the drawpiece formed in run 20.

Figure 6 presents the vertical and horizontal force components and the COF for Eq. (1) during the formation time for run 17. Four stages can be designated for the plot. Stage I – pre-forming, when the tool initializes contact with the sheet. In this part, unstable conditions do not allow proper estimation of the COF. Stage II – stabilizing forming conditions. In this stage, the tool plunges until it reaches full contact depth and the forming temperature also stabilizes. Stage III – the process is under steady conditions. This part is suitable for measuring the COF during the ISF process. Stage IV – unstable tool retraction

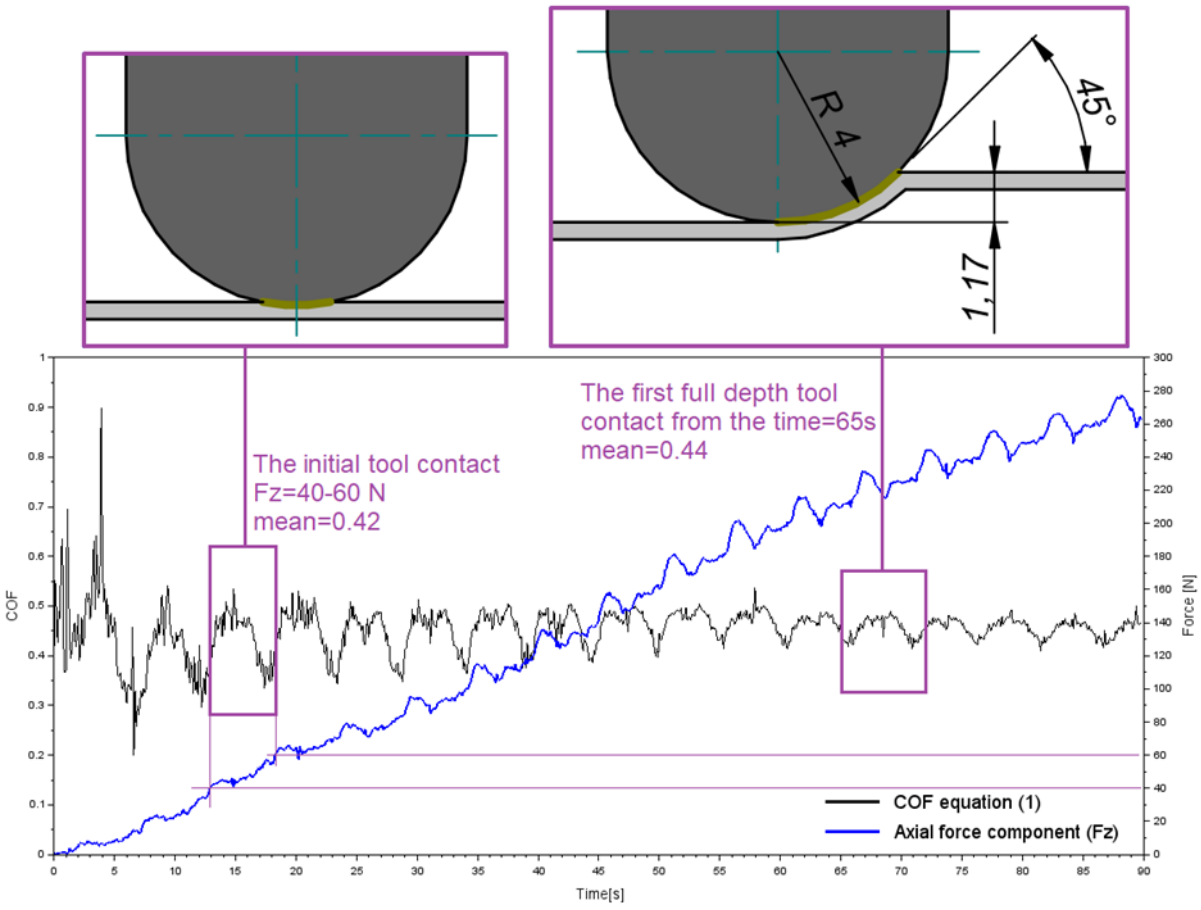

Figure 8. Zoomed area of Figure 7 beginning for the Eq.(1) where initial contact (COF=0.42) and the first full contact depth of the tool (COF = 0.44) exist.

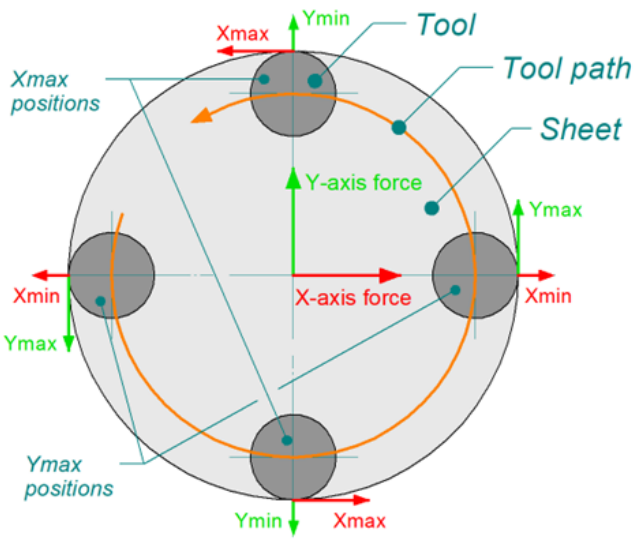

Figure 9. Extreme horizontal force components with respect to the tool position.

conditions. In this part of the path, the tool requires high acceleration values from the machine axis due to the tool path restricting it until it reaches the drawpiece axis. The last peak on the plot in this stage represents an overlap of the tool with the drawpiece radius. In that area, measurement of COF value may be burdened with error caused by vibration of the entire instrumentation and unstable conditions. This part shouldn't be considered into analysis. The mean values of the COF listed in Table 5 have been determined for the stabilized forming conditions (Stage II) and steady conditions of the COF (Stage III).

In the next step, both equations (1) and (2) were applied in the extraction of COF values from the acquired data. Figure 7 presents the calculated COFs in forming period time for run #17 under steady conditions. The difference in the whole experiment between equations (1) and (2) fluctuate from 0.18 to 0.2 for stage III (stabilized forming conditions).

To observe the differences between COF in the initial tool contact and the first full-depth tool, several COF data were analyzed. As an example, Run #17 was presented. The COF plot for Eq.(1) was cut to 90 seconds and both types of contact were examined. Initial tool contact was determined as the axial force component range from 40 N to 60 N. For the forming parameters feed rate 2000 mm/min and incremental step depth 0.1 mm, the tool will achieve the first full depth contact after 65 s from the beginning of the forming. Figure 8 shows the difference between both contacts. The differences for the runs were less than 0.04 and may be considered negligible comparing to discrepancy up to 0.39 between the COFs: initial tool contact and stabilized forming.

Determination of the COF using only one horizontal force component was also investigated for the stabilized forming region. Four extreme tool locations can be established, two where the X-axis force component exceeds the maximum and two for the Y-axis (Figure 9). By selecting only these extreme components of the horizontal force measurements, the COF was estimated (Figures 10 and 11).

For the current experiment, the significance of the regression model was evaluated by calculating the statistics F at a p-value = 0.05 and correlation level 0.7. This means if p-value of the created model is higher than 0.05, the model should be rejected. The correlation level above 0.7 means that there is a significant correlation. A simple correlation test was executed between the results of the experiment. A low interaction was found between spindle speed, tool feed, incremental step depth and COF responses. However, high correlation values were observed between the COF Eq. (1) Initial contact, Stabilized forming: COF Eq. (1), COF Eq. (2), Xmax COF and Ymax COF (Figure 12).

In the next step, an analysis of variance (ANOVA) was performed for the COF values obtained to examine the influence of factors such as spindle speed, tool feed and incremental step depth on the COF output. At the beginning, four models were summarized: quadratic, two-factor interaction (2FI), linear and mean (Table 6).

However, only the mean model was characterized by a p-value less than 0.05. The quadratic model seems to be the next model to consider, but this model will be aliased, which means that it cannot accurately fit this design and should not be considered for analysis. A trail of quadratic model applications was performed. The ANOVA for the quadratic model is shown in Table 7. The model F-value of 4.64 means the model is not significant in relation to the noise. A backward elimination algorithm was applied. This procedure discards input factors whose p-value exceeds more than 0.05, starting with the highest model sources. This elimination may improve the total p-value of the model. However, the algorithm eliminated all input factors that remained at the mean model level.

Finally, the mean model was used for each COF response (Table 5). A sequential p-value higher than 0.05 for the rest of the summarized models informs that each of the input factors (spindle speed, incremental step depth, step size) is not significant for the COF result in the experimental range.

4. Conclusions

In this paper, the COF between a tungsten carbide tool and a grade 2 titanium sheet was investigated during the SPIF process. A central composite design was analyzed. The following conclusions can be drawn from the research:

- The input factors included in the experiment, such as: spindle speed, feed rate and incremental step depth in the selected range of the research, have no effect on the COF value by both presented equations and measured in the two stages of forming or on the Xmax COF and Ymax COF.
- The four zones for the COF plot can be specified: I – tool approach stage, II – forming process stabilisation, III– stable forming zone, IV – tool

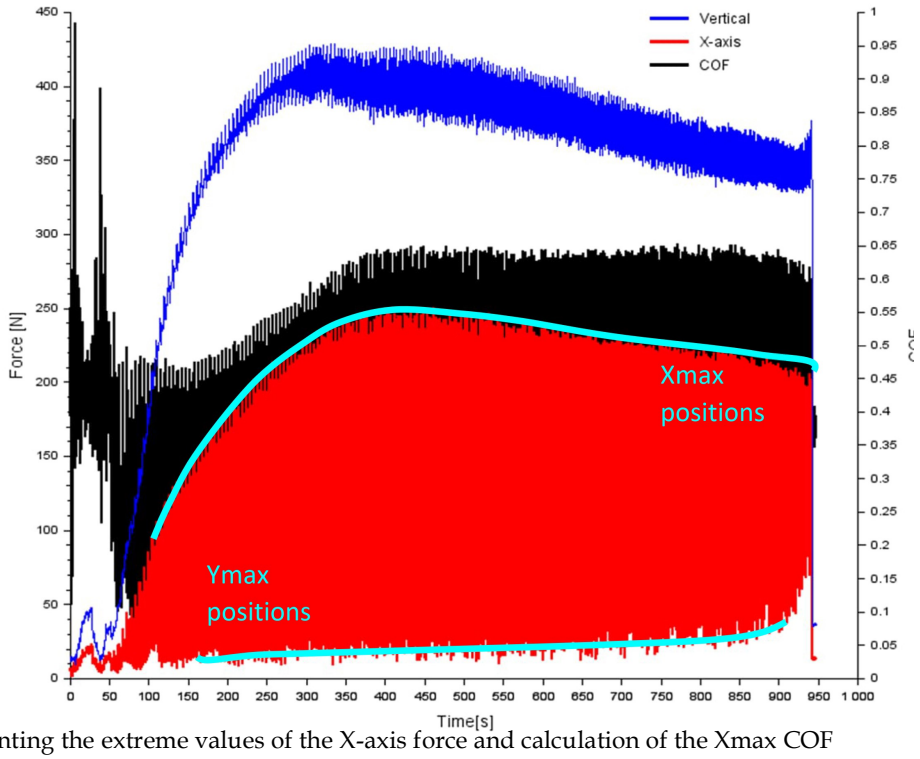

Figure 10. Plot presenting the extreme values of the X-axis force and calculation of the Xmax COF

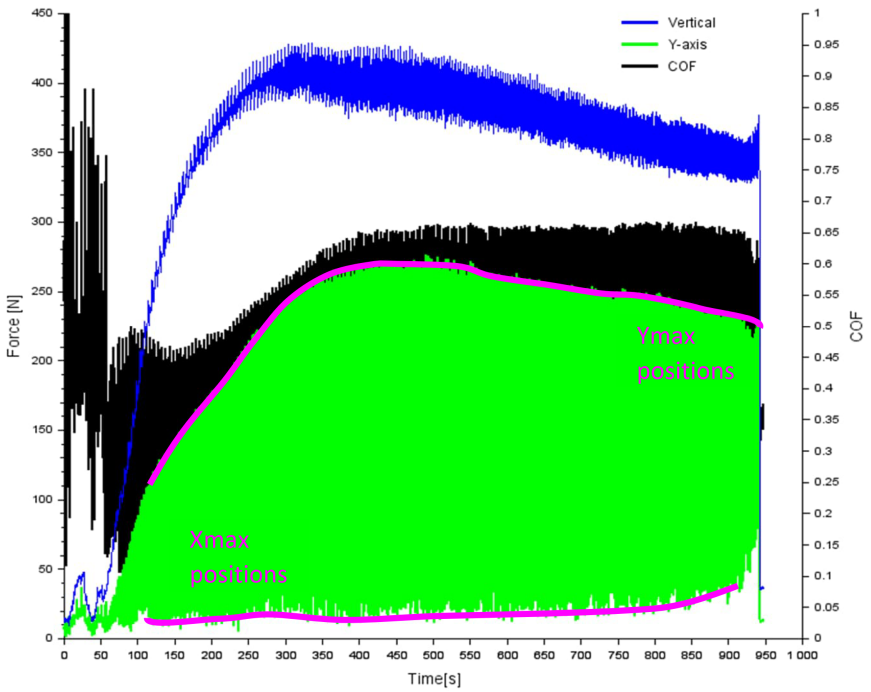

Figure 11. Plot presenting the extreme values of the Y-axis force and calculation of the Ymax COF

retraction stage.

- The III zone seems to be the most favorable for estimating COF values due to stabilization of the forming conditions. Zone II can also be used for the COF estimation during initial contact between the tool and sheet. Zones I and IV should be excluded from the analysis due to very unstable conditions (the tool approach and retract).
- High correlation values were found between the response outputs in the stabilized forming area: COF, Xmax COF and Ymax COF (R2 = 0.997 up to R2 = 0.999), which implies that only one horizontal force component with a vertical force component may be enough to estimate the COF in the SPIF

	Run	A:Spindle speed	B:Tool feed	C:Incremental step depth	COF Eq. (1) Initial stage	COF Eq. (1) Stabilized forming	COF Eq. (2) Stabilized forming	COF Eq. (1) Xmax	COF Eq. (1) Ymax
Run	1.000	-0.222	0.031	-0.220	0.119	0.356	0.357	0.370	0.375
A:Spindle speed	-0.222	1.000	0.036	0.000	-0.301	-0.226	-0.244	-0.216	-0.215
B:Tool feed	0.031	0.036	1.000	0.000	0.124	-0.117	-0.104	-0.120	-0.117
C:Incremental step depth	-0.220	0.000	0.000	1.000	-0.160	0.133	0.131	0.128	0.125
COF Eq. (1) Initial stage	0.119	-0.301	0.124	-0.160	1.000	-0.217	-0.218	-0.206	-0.199
COF Eq. (1) Stabilized forming	0.356	-0.226	-0.117	0.133	-0.217	1.000	0.999	0.999	0.999
COF Eq. (2) Stabilized forming	0.357	-0.244	-0.104	0.131	-0.218	0.999	1.000	0.998	0.997
COF Eq. (1) Xmax	0.370	-0.216	-0.120	0.128	-0.206	0.999	0.998	1.000	1.000
COF Eq. (1) Ymax	0.375	-0.215	-0.117	0.125	-0.199	0.999	0.997	1.000	1.000

Figure 12. Correlation test results.

Table 6. Fit summary for comparison of the different models

Source	Sequential p-value	Adjusted R^2	Predicted R^2	Decision
Mean	< 0.0001			Selected
Linear	0.6027	-0.1043	-1.2172	
2FI	0.5162	-0.1622		
Quadratic	0.0532	0.7259		Aliased - check

process.

- The mean COF value for Eq. (1) initial contact is 0.4 with a standard deviation of 0.074, for Eq. (1) stabilized forming obtained in the analysis of both the vertical and horizontal forces is 0.656 with a standard deviation of 0.036, while the mean COF for the Eq. (2) stabilized forming achieves 0.469 with 0.043 standard deviation, Xmax horizontal component the Xmax COF = 0.669 with a standard deviation of 0.041 and for the Ymax component it is 0.668 with a standard deviation of 0.043.
- The differences between the COF Eq. (1) initial contact and COF Eq. (1) the first full tool depth contact (0.04) may be insignificant compared to the COF Eq. (1) stabilized forming. The difference in those COF reach up to 0.39. The authors suppose that these apparent discrepancies result from the temperature variation in a tool-workpiece contact zone. However this hypothesis must be validated in the future by proper measurements or FEM analysis.

Future research should focus on finite model analysis with regard to the COF obtained. Forming conditions should be compared in terms of the forming forces and the shape accuracy achieved. In addition, different tool shapes should be considered in the analysis as well as different drawpiece angles and lubrication types.

Table 7. ANOVA table for the quadratic COF equation (1) Stabilized forming model

Source	Sum of squares	Degrees of freedom	Mean square	F-value	p-value
Model	0.0134	8	0.0017	4.64	0.1170
A-Spindle speed	0.0051	1	0.0051	14.11	0.0330
B-Tool feed	0.0004	1	0.0004	1.23	0.3491
C-Incremental step depth	0.0018	1	0.0018	5.00	0.1114
AB	0.0041	1	0.0041	11.32	0.0436
AC	0.0018	1	0.0018	5.00	0.1114
BC	0.0048	1	0.0048	13.30	0.0356
A^2	0.0028	1	0.0028	7.86	0.0677
B^2	0.0029	1	0.0029	8.15	0.0648
C^2	0.0000	0			
Residual	0.0011	3	0.0004		
Correlation total	0.0145	11			

Table 8. Mean models for COF responses

Response	Model	Observations	Minimum	Maximum	Mean	Standard deviation
COF Eq. (1) Initial contact	Mean	20	0.28	0.56	0.4	0.074
COF Eq. (1) Stabilized forming	Mean	12	0.6	0.72	0.656	0.036
COF Eq. (2) Stabilized forming	Mean	12	0.4	0.54	0.469	0.043
Xmax COF Eq. (1)	Mean	12	0.61	0.74	0.669	0.041
Ymax COF Eq. (1)	Mean	12	0.61	0.74	0.668	0.043

References

1. Oleksik, V.; Trzepieciński, T.; Szpunar, M.; Chodoła, Ł.; Ficek, D.; Szczęsny, I. Single-Point Incremental Forming of Titanium and Titanium Alloy Sheets. Materials 2021, 14, 6372. https://doi.org/10.3390/ma14216372
2. Trzepieciński, T.; Krasowski, B.; Kubit, A.; Wydrzyński, D. Possibilities of Application of Incremental Sheet-Forming Technique in Aircraft Industry. Sci. Lett. Rzesz. Univ. Technol. - Mech. 2018, 90(1), 87-100. https://doi.org/10.7862/rm.2018.08
3. Trzepieciński, T.; Najm, S.M.; Sbayti, M.; Belhadjsalah, H.; Szpunar, M.; Lemu, H.G. New Advances and Future Possibilities in Forming Technology of Hybrid Metal-Polymer Composites Used in Aerospace Applications. Journal of Composites Science 2021, 5(8), 217. https://doi.org/10.3390/jcs5080217
4. Rosca, N.; Oleksik, M.; Oleksik, M. Experimental Study Regarding PA and PE Sheets on Single Point Incremental Forming Process. MATEC Web of Conferences 2021, 343, 03009. https://doi.org/10.1051/matecconf/202134303009
5. Harhash, M.; Palkowski, H. Incremental sheet forming of steel/polymer/steel sandwich composites. Journals of Materials Research and Technology 2021, 13, 417-430. https://

doi.org/10.1016/j.jmrt.2021.04.088

6. Kharche, A.; Barve, S. Incremental sheet forming of composite material. Materials Today: Proceedings 2022, 63, 176-184. https://doi.org/10.1016/j.matpr.2022.02.447
7. Jadhav S., Goebel R., Homberg W., Kleiner M. Process optimization and control for incremental forming sheet metal forming. Proceedings of the Conference of the International Deep Drawing Research Group, Bled, Slovenia, 11-15 May 2003, pp. 165-171.
8. Cheng, Z.; Li, Y.; Xu, C.; Liu, Y.; Ghafoor, S.; Li, F. Incremental sheet forming towards biomedical implants: a review. Journal of Materials Research and Technology 2020, 9(4), 7225-7251. https://doi.org/10.1016/j.jmrt.2020.04.096
9. Patel, D.; Gandhi, A. A review article on process parameters affecting Incremental Sheet Forming (ISF). Materials Today: Proceedings 2022, 63, 368-375. https://doi.org/10.1016/j.matpr.2022.03.208
10. Harfoush, A.; Haapala, K.R.; Tabei, A. Application of Artificial Intelligence in Incremental Sheet Metal Forming: A Review. Procedia Manufacturing 2021, 53, 606-617. https://doi.org/10.1016/j.promfg.2021.06.061
11. Duflou, J.R.; Habraken, A.M.; Cao, J.; Malhotra, R.; Bambach, M.; Adams, D.; Vanhove, H.; Mohammadi, A.; Jeswiet, J. Single point incremental forming: state-of-the-art and prospects. International Journal of Materials Forming 2018, 11, 743-773. https://doi.org/10.1007/s12289-017-1387-y
12. Trzepieciński, T.; Szpunar, M.; Dzierwa, A.; Żaba, K. Investigation of Surface Roughness in Incremental Sheet Forming of Conical Drawpieces from Pure Titanium Sheets. Materials 2022, 15, 4278. https://doi.org/10.3390/ma15124278
13. Więckowski, W.; Adamus, J.; Dyner, M.; Motyka, M. Tribological Aspects of Sheet Titanium Forming. Materials 2023, 16, 2224. https://doi.org/10.3390/ma16062224
14. Szewczyk, M.; Szwajka, K. Assessment of the Tribological Performance of Bio-Based Lubricants Using Analysis of Variance. Advances in Mechanical and Materials Engineering 2023, 40, 31-38. https://doi.org/10.7862/rm.2023.4
15. Trzepieciński T., Oleksik V., Pepelnjak T., Najm S.M., Paniti I., Maji K, Emerging Trends in Single Point Incremental Sheet Forming of Lightweight Metals. Metals 2021, 11(8), 1188. https://doi.org/10.3390/met11081188
16. Najm, S.M.; Paniti, I.; Trzepieciński, T.; Nama, S.A.; Viharos, Z.J.; Jacso, A. Parametric Effects of Single Point Incremental Forming on Hardness of AA1100 Aluminium Alloy Sheets. Materials 2021, 14(23), 7263. https://doi.org/10.3390/ma14237263
17. Najm, S.M.; Paniti, I. Study on Effecting Parameters of Flat and Hemispherical end Tools in SPIF of Aluminium Foils. Technical Gazette 2020, 27(6), 1844-1849. https://doi.org/10.17559/TV-20190513181910
18. Trzepieciński T., Najm S.M., Oleksik V., Vasilca D., Paniti I., Szpunar M. Recent developments and future challenges in incremental sheet forming of aluminium and aluminium alloy sheets. Metals 2022, 12(1), 124. https://doi.org/10.3390/met12010124
19. Sbayti, M.; Bahloul, R.; Belhadjasalah, H. Efficiency of optimization algorithms on the adjustment of process parameters for geometric accuracy enhancement of denture plate in single point incremental sheet forming. Neural Computing and Applications 2020, 32, 8829-8846. https://doi.org/10.1007/s00521-019-04354-y
20. Martins, P.A.F.; Bay, N.; Skjoedt, M.; Silva, M.B. Theory of single point incremental forming. CIRP Annals 2008, 57(1), 247-252. https://doi.org/10.1016/j.cirp.2008.03.047
21. Pepelnjak, T.; Sevšek, L.; Lužanin, O.; Milutinović, M. Finite Element Simplifications and Simulation Reliability in Single Point Incremental Forming. Materials 2022, 15, 3707. https://doi.org/10.3390/ma15103707
22. Gulati V., Aryal A., Katyal P., Goswami A. Process parameters optimization in single point incremental forming. Journal of The Institution of Engineers (India): Series C 2016, 97(2), 185-193. https://doi.org/10.1007/s40032-015-0203-z
23. Wei, H.; Hussain, G.; Iqbal, A.; Zhang, Z.P. Surface Roughness as the Function of Friction Indicator and an Important Parameters-Combination Having Controlling Influence on the Roughness: Recent Results in Incremental Forming. International Journal of Advanced Manufacturing Technology 2019, 101, 2533-2545. https://doi.org/10.1007/s00170-018-3096-1
24. Cai, S.; Wu, R.; Wang, Z.; Li, M.; Chen, J. Numerical Simulation of Friction Stir-Assisted Incremental Forming with Synchronous Bonding of Heterogeneous Sheet Metals. International Journal of Advanced Manufacturing Technology 2020, 106, 2747-2763. https://doi.org/10.1007/s00170-019-04792-x
25. Patel, J.R.; Samvatsar, K.S.; Prajapati, H.P.; Rangrej, S.S. Optimization of process parameters for reducing surface roughness produced during single point incremental forming process. International Journal on Recent Technologies in Mechanical and Electrical Engineering 2015, 2(9), 19-23. http://dx.doi.org/10.6084/M9.FIGSHARE.12578372.V1

26. Xu, Q.; Yao, Z. Forming Parameters on Friction during Single Point Incremental Forming. Advances in Materials Science and Engineering 2022, 2022, e7534196. https://doi.org/10.1155/2022/7534196
27. Najm, S.M.; Paniti, I. Artificial neural network for modeling and investigating the effects of forming tool characteristics on the accuracy and formability of thin aluminum alloy blanks when using SPIF. International Journal of Advanced Manufacturing Technology 2021, 114, 2591-2615. https://doi.org/10.1007/s00170-021-06712-4
28. Milutinović, M.; Lendjel, R.; Baloš, S.; Zlatanović, D.L.; Sevšek, L.; Pepelnjak, T. Characterisation of geometrical and physical properties of a stainless steel denture framework manufactured by single-point incremental forming. Journal of Materials Research and Technology 2021, 10, 605-623. https://doi.org/10.1016/j.jmrt.2020.12.014
29. Sbayti, M.; Ghiotti, A.; Bahloul, R.; BelhadjSalah, H.; Bruschi, S. Effective strategies of metamodeling and optimization of hot incremental sheet forming process of Ti6Al4V artificial hip joint component. Journal of Computational Science 2022, 60, 101595. https://doi.org/10.1016/j.jocs.2022.101595
30. Popp, M.; Rusu, G.; Racz, S.G.; Oleksik, V. Common defects of parts manufactured through single point incremental forming. MATEC Web of Conferences 2021, 343, 04007. https://doi.org/10.1051/matecconf/202134304007
31. Rosca, N.; Oleksik, V.; Pascu, A.; Oleksik, M.; Avrigean, E. Optical study for springback prediction, thickness reduction and forces variations on single point incremental forming. Materials Today: Proceedings 2019, 12, 213-218. https://doi.org/10.1016/j.matpr.2019.03.116
32. Hussain, G.; Gao, L.; Zhang, Z.Y. Formability Evaluation of a Pure Titanium Sheet in the Cold Incremental Forming Process. Int. J. Adv. Manuf. Technol. 2008, 37, 920-926. https://doi.org/10.1007/s00170-007-1043-7
33. ajay, C.V. Parameter Optimization in Incremental Forming of Titanium Alloy Material. Trans. Indian Inst. Met. 2020, 73, 2403-2413. https://doi.org/10.1007/s12666-020-02044-1
34. Szpunar, M.; Trzepieciński, T.; Ostrowski, R.; Zwolak, M. Research on Forming Parameters Optimization of Incremental Sheet Forming Processf or Commercially Pure Titanium Grade 2 Sheets. Arch. Metall. Mater. 2022 Vol 67 No 4 1411-1418 2022. http://dx.doi.org/10.24425/amm.2022.141068
35. Kumar, R.; Kumar, G.; Singh, A. An Assessment of Residual Stresses and Micro-Structure during Single Point Incremental Forming of Commercially Pure Titanium Used in Biomedical Applications. Mater. Today Proc. 2020, 28, 1261-1266. https://doi.org/10.1016/j.matpr.2020.04.147
36. Mishra, S.; Yazar, K.U.; Kar, A.; Lingam, R.; Reddy, N.V.; Prakash, O.; Suwas, S. Texture and Microstructure Evolution During Single-Point Incremental Forming of Commercially Pure Titanium. Metall. Mater. Trans. A 2021, 52, 151-166. https://doi.org/10.1007/s11661-020-06000-y
37. Yoganjaneyulu, G.; Vigneshwaran, S.; Palanivel, R.; Alblawi, A.; Rasheed, M.A.; Laubscher, R.F. Effect of Tool Rotational Speed on the Microstructure and Associated Mechanical Properties of Incrementally Formed Commercially Pure Titanium. J. Mater. Eng. Perform. 2021, 30, 7636-7644. https://doi.org/10.1007/s11665-021-05900-3
38. Decultot, N.: Formage incrémental de tôle d'aluminium : étude du procédé à l'aide de la mesure de champs et identification de modèles de comportement, Universite de Toulouse, 2011.
39. Saidi, B.; Boulila, A.; Ayadi, M.; Nasri, R. Prediction of the Friction Coefficient of the Incremental Sheet Forming SPIF. In Proceedings of the 6th International Congress Design and Modelling of Mechanical Systems CMSM'2015, Hammamet, Tunisia, 23-25 March 2015.
40. Shin, J. Investigation of Incremental Sheet Forming (ISF) Using Advanced Numerical and Analytical Approaches. Thesis, 2021.
41. Durante, M.; Formisano, A.; Langella, A.; Capece Minutolo, F.M. The Influence of Tool Rotation on an Incremental Forming Process. J. Mater. Process. Technol. 2009, 209, 4621-4626. https://doi.org/10.1016/j.jmatprotec.2008.11.028
42. Hamilton, K.A.S. Friction and External Surface Roughness in Single Point Incremental Forming: A Study of Surface Friction, Contact Area and the 'Orange Peel' Effect. thesis, 2010.
43. Li, Y.; Liu, Z.; Daniel, W.J.T. (Bill); Meehan, P.A. Simulation and Experimental Observations of Effect of Different Contact Interfaces on the Incremental Sheet Forming Process. Mater. Manuf. Process. 2014, 29, 121-128. https://doi.org/10.1080/10426914.2013.822977
44. Xu, Q.; Yao, Z. Forming Parameters on Friction during Single Point Incremental Forming. Adv. Mater. Sci. Eng. 2022, 2022, e7534196. https://doi.org/10.1155/2022/7534196
45. Akhavan Farid, A.; Foong, S.S.; Krejcar, O.; Namazi, H. Complexity-Based Analysis of the Effect of Forming Parameters on the Surface Finish of Workpiece in Single Point Incremental Forming (SPIF). Fractal Fract. 2021, 5, 241. https://doi.org/10.3390/fractalfract5040241